Applied Energy 219 (2018) 408–424

Contents lists available at ScienceDirect

Applied Energy

journal homepage: www.elsevier.com/locate/apenergy

Optimal design of multi-energy systems with seasonal storage

Paolo Gabrielli[a], Matteo Gazzani[b], Emanuele Martelli[c], Marco Mazzotti[a,*]

[a] Institute of Process Engineering, ETH Zurich, Sonneggstrasse 3, 8092 Zurich, CH, Switzerland
[b] Copernicus Institute of Sustainable Development, Utrecht University, Heidelberglaan 2, 3584 CS Utrecht, NL, The Netherlands
[c] Department of Energy, Politecnico di Milano, Via Lambruschini 4, 20156 Milano, IT, Italy

HIGHLIGHTS

- Novel MILP approaches to enable design of MES including seasonal energy storage.
- Good accuracy and much lower computational complexity compared to current approaches.
- Realistic Swiss case-study evaluated in terms of total annual cost and emissions.
- Extensive sensitivity analysis defining design guidelines for seasonal energy storage.

ARTICLE INFO

Keywords:
Multi-energy systems
Microgrids
Seasonal storage
Investment planning
Yearly scheduling
MILP
Power-to-gas

ABSTRACT

Optimal design and operation of multi-energy systems involving seasonal energy storage are often hindered by the complexity of the optimization problem. Indeed, the description of seasonal cycles requires a year-long time horizon, while the system operation calls for hourly resolution; this turns into a large number of decision variables, including binary variables, when large systems are analyzed. This work presents novel mixed integer linear program methodologies that allow considering a year time horizon with hour resolution while significantly reducing the complexity of the optimization problem. First, the validity of the proposed techniques is tested by considering a simple system that can be solved in a reasonable computational time without resorting to design days. Findings show that the results of the proposed approaches are in good agreement with the full-scale optimization, thus allowing to correctly size the energy storage and to operate the system with a long-term policy, while significantly simplifying the optimization problem. Furthermore, the developed methodology is adopted to design a multi-energy system based on a neighborhood in Zurich, Switzerland, which is optimized in terms of total annual costs and carbon dioxide emissions. Finally the system behavior is revealed by performing a sensitivity analysis on different features of the energy system and by looking at the topology of the energy hub along the Pareto sets.

1. Introduction

Recently, the energy sector has been riding a wave of grand transformation: the necessity of decreasing the environmental impact has led to the deployment of conversion and storage technologies based on renewable energy sources [1]. In this context, multi-energy systems (MES) represent a new paradigm which exploits the interaction between various energy carriers (e.g. electricity and heat) at design and operation phase, allowing for improved technical, economic and environmental performance of the system [2]. Within this framework, seasonal storage systems have recently caught much attention due to their ability to compensate the seasonal intermittency of renewable energy sources [3]. However, compensating renewables fluctuations at the seasonal scale is particularly challenging: on the one hand, a few systems, such as hydrogen storage and large thermal storage, allow offsetting seasonal variations in renewable energy generation; on the other hand, the optimal design and operation is complicated by the large number of decision variables, due to the required length and resolution of the time horizon.

Several works provide comprehensive reviews of the model formulations and computer tools adopted for investigating MES and their integration with renewable energy sources and storage technologies. For instance, Alarcon-Rodriguez et al. focused on the multi-objective planning of distributed energy resources [4]; Connolly et al. presented a review of the computer tools implemented for analyzing the integration of renewable energy into various energy systems [5], whereas Keirstead

* Corresponding author.
E-mail address: marco.mazzotti@ipe.mavt.ethz.ch (M. Mazzotti).

http://dx.doi.org/10.1016/j.apenergy.2017.07.142
Received 25 May 2017; Received in revised form 19 June 2017; Accepted 31 July 2017
Available online 05 October 2017

Nomenclature

A	available area for solar installation (m^2)
a	binary variable for technology selection (–)
b	binary variable for technology selection (–)
D	number of design days (–)
d	design day index
E	stored energy (kWh)
e	annual CO_2 emission (ton_{CO_2}/yr)
F	input power (kW)
I	solar radiation (kWh/m^2)
i	technology index
J	annual cost (€/yr)
j	carrier index
K	length of the time horizon (hour of the day)
k	time index (hour of the day)
L	user demand (kW)
$\mathscr{M}$	set of available technologies
M	number of available technologies (–)
$\mathscr{N}$	set of available carriers
P	output power (kW)
Q	thermal output power (kW)
S	technology size (kW)
T	length of the time horizon (hour of the year)
t	time index (hour of the year)
U	import power (kW)
u	import price (€/kWh)
V	export power (kW)
v	export price (€/kWh)
w	binary variable for capital cost calculation (–)
x	binary variable for on/off status (–)
Y	length of the time horizon (day of the year)
y	time index (day of the year)

Greek letters

α	efficiency coefficient (–)
β	efficiency coefficient (–)
γ	efficiency coefficient (kW)
Δ	time variation (h)
δ	size coefficient (–)
ε	specific emission coefficient (ton_{CO_2}/kWh)
ζ	size coefficient (kW)
η	conversion or storage efficiency (–)
Θ	air temperature (°C)
θ	cost coefficient (–)
κ	size coefficient (–)
Λ	storage loss coefficient (h^{-1})
λ	cost coefficient (–)
μ	cost coefficient (€)
ν	size coefficient (kW)
Π	storage loss coefficient (–)
ρ	first principle-to-electrical efficiency ratio (–)
σ	sequence of design days along the year (–)
τ	storage charging/discharging time (h)

Subscripts

A	subset of technologies
B	subset of technologies
c	capital cost
e	electricity
g	natural gas
h	heat
m	maintenance cost
o	operation cost
S	subset of technologies

Superscripts

A	subset of decision variables
B	subset of decision variables
int	intermediate
max	maximum
min	minimum

Acronym

COP	coefficient of performance
CS	conventional scenario
edHP	electricity-driven heat pump
FC	fuel cell
FSO	full scale optimization
HS	hydrogen storage
HWTS	hot water sensible thermal storage
LiB	lithium battery
M0	method 0
M1	method 1
M2	method 2
MES	multi-energy system
MGT	micro gas turbine
MILP	mixed integer linear program
NG	natural gas
PEME	proton exchange membrane electrolyzer
PEMFC	proton exchange membrane fuel cell
PtG	power to gas
PV	photovoltaic
PWA	piecewise affine
SOFC	solid oxide fuel cell
TS	thermal solar

et al. [6] and Allegrini et al. [7] focused on urban energy system models; Mancarella provided an overview of concepts and models for the planning and analysis of multi-energy systems [2]. When storage technologies are available, the optimal design of MES is significantly complicated by the necessity to consider the system operation already at design phase to accurately make use of the storage systems. Although a few nonlinear approaches have been proposed, for instance by Elsido et al. [8], mixed-integer linear programming (MILP) has been particularly favored as optimization framework for MES design and operation since it catches well the features of the system with a reasonable computational complexity. The problem of optimal technology selection and unit commitment through MILP formulation has been extensively investigated in the past. For example, Marnay et al. presented the case of a commercial building micro-grid with heat and electrical storage [9]; Hawkes and Leach extended the study by considering a hospital and residential buildings [10]. Later, Angrisani et al. investigated the energy, economic, and environmental performance of micro tri-generation systems [11]. Fazlollahi et al. introduced methods for multi-objective design of complex energy systems [12], and Ahmadi et al. presented the thermodynamic modeling and multi-objective optimization of an energy system for the simultaneous generation of electricity, heating, cooling and hot water [13]. Whereas these works were mainly focused on small, yet centralized systems (i.e. one hub for different end users), a number of studies also investigated energy distribution among the different nodes of decentralized energy systems (i.e. multiple hubs for different end users). For example, Genon et al.

presented the environmental assessment of small district heating systems [14], while Weber and Shah optimized the structure of the heating network in addition to technology selection and unit dispatch [15]. Furthermore, various case-studies have been proposed by applying such tools: Mehleri et al. investigated the optimal design and operation of different neighborhoods within the Greek energy sector [16,17]; Omu et al. focused on the possible measures to reduce the carbon footprint of the UK energy sector [18], and Bracco et al. presented the design and operation of the micro-grid built at the University campus in Savona, Italy [19]. Finally, the interest in multi-energy systems at different levels (from residential to national) has triggered the development of commercial tools for MILP formulation. These include EnergyPlan, an optimization tool developed at Aalborg University, which simulates the operation of national energy systems [20], and DER-CAM, developed by the Lawrence Berkeley National Laboratory [21]. Recent improvements of DER-CAM tool include building retrofitting [22] and detailed models of sensible thermal storage systems [23].

In these works, the remarkable complexity of the optimization problem required significant model simplifications. In specific, all these past studies considered a one-year time horizon based on design days. Recently, Elsido et al. investigated the weekly periodicity in the operation of CHP units with thermal storage, describing the entire year through typical weeks [8]. These approaches are suitable when analyzing intraday storage installation and operation, whilst they are not able to describe seasonal operation cycles due to the discontinuity between the selected design days (or weeks). Longer time horizons have been considered when investigating only the operation of multi-energy systems, e.g. in [24], but not at design phase.

This work aims at addressing and overcoming this issue. To this end, two novel MILP formulations based on the coupling of typical design days and on the distinction between two groups of decision variables are proposed. These approaches allow considering an hour resolution of the entire year while maintaining a low number of binary variables, thus enabling the solution of complex systems featuring seasonal energy storage. In the following, first, the proposed techniques are tested by considering a simple system that can be solved in a reasonable computational time without resorting to design days (i.e. year time horizon with full hourly resolution). Next, the presented methodology is applied to a residential multi-energy system based on a neighborhood in Zurich, Switzerland: different hub designs are determined and analyzed to minimize the total annual cost and CO_2 emissions. Finally, the operation of the energy storage during the whole year is presented and discussed.

The paper is structured as follows. Section 2 describes the features of the investigated multi-energy system, formulates the traditional optimization problem and describes the novel approaches. Section 3 presents the results. Finally, in Section 4 conclusions are drawn.

2. System description and formulation of the optimization problem

The multi-energy system considered in this study has the primary objective of supplying the energy demanded by a specified user. The MES is connected to the gas and electrical grids and includes a set of conversion technologies, both traditional and renewable-based, and of storage units. Fig. 1 provides a schematic representation of such a system. The weather conditions, electricity and gas prices, and energy demand profiles are the three sets of inputs to the optimization problem. The model returns the optimal system design in terms of technology selection and size, and the optimal operation of the installed units.

The problem is mathematically formulated as a MILP, where binary variables are introduced to model the performance of the conversion units, and the capital cost of the investigated technologies. The MILP can be written in general form as

$$\begin{aligned} &\min_{\mathbf{x},\mathbf{y}} \ (\mathbf{c}^T\mathbf{x} + \mathbf{d}^T\mathbf{y}) \\ &\text{s.t.} \\ &\boldsymbol{A}\mathbf{x} + \boldsymbol{B}\mathbf{y} = \mathbf{b} \\ &\mathbf{x} \geqslant \mathbf{0} \in \mathbb{R}^{N_x}, \mathbf{y} \in \{0,1\}^{N_y} \end{aligned} \tag{1}$$

where $\mathbf{c}$ and $\mathbf{d}$ represent the cost vectors associated to continuous and binary decision variables, $\mathbf{x}$ and $\mathbf{y}$ respectively; $\boldsymbol{A}$ and $\boldsymbol{B}$ are the corresponding constraint matrices and $\mathbf{b}$ is the constraint known-term; N_x and N_y indicate the dimension of $\mathbf{x}$ and $\mathbf{y}$, respectively. In the following, the optimization problem is described in detail in terms of input data, decision variables, constraints, and objective function.

2.1. Input data

The input data are time-dependent profiles for 2016 in a fraction of Altstetten, a neighborhood within the city of Zurich, Switzerland, which features a peak electricity demand of 0.43 MW and a peak thermal demand of 2 MW. The hour profiles for all input data are reported in the appendix. Data are assumed to be constant along the lifetime of the

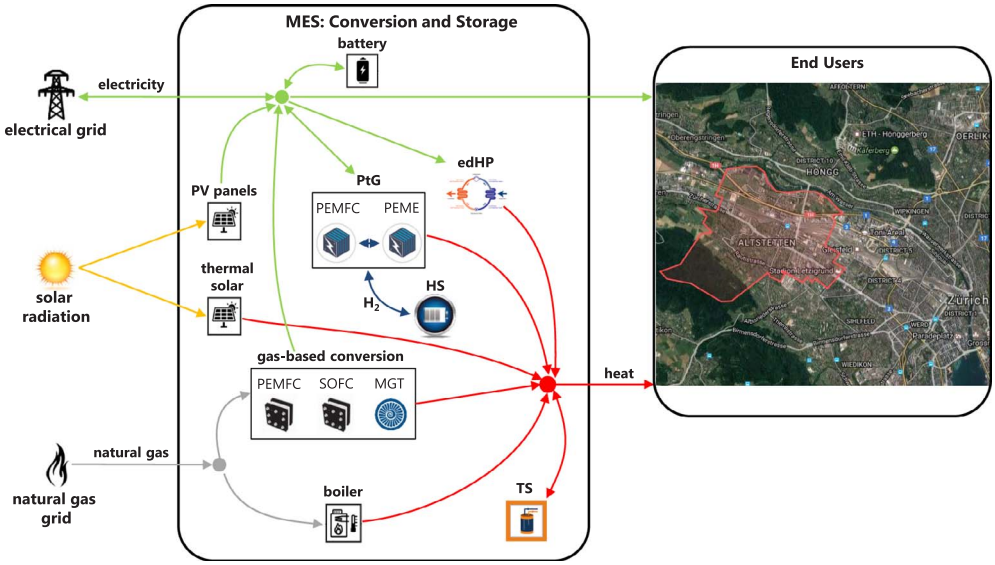

Fig. 1. Schematic representation of the investigated multi-energy system.

system and known without uncertainty, i.e. it is assumed that the possible realizations of the uncertainty and the evolution of the demand profiles are represented by the historical data. Indeed, the optimization of MES considering the uncertainties of the input data (e.g. electricity price, heat and electricity demand, renewable potential) is an important and open topic, which is being tackled by several researchers by means of different methodologies (e.g. [25–32]). However, such research activity is not within the scope of this paper, which aims at providing a MILP framework for implementing seasonal storage, regardless of the extent to which input data are representative of the future. Moreover, findings of this work can be extended and implemented in optimization problems under uncertainties. In this framework, solving the optimization problem at every time instant of the time horizon, i.e. every hour of the year, provides the optimal solution to the problem.

In our MILP implementation, inputs to the optimization problem are:

i. The expected weather conditions, namely air temperature, $\boldsymbol{\Theta} \in \mathbb{R}^T$, and solar radiation, $\mathbf{I} \in \mathbb{R}^T$, where T indicates the length of the time horizon. Data are available at every hour of the year, hence $T = 8760$.
ii. The expected prices of energy utilities, namely import prices, $\mathbf{u}_e$ and $\mathbf{u}_g \in \mathbb{R}^T$, for electricity and gas, respectively, and export electricity price, $\mathbf{v}_e \in \mathbb{R}^{M\times T}$, variable for different technologies, where M indicates the number of available technologies. While the import gas price is considered to be fixed along the year, the import electricity price is not constant. Notably, the electricity price features a very volatile profile, which is the result of a complex market regulation together with a broad portfolio of electricity suppliers (i.e. renewables-, nuclear-, fossil fuel-based). The Swiss electricity spot market price for 2016 with an hourly resolution is considered.
iii. The expected electricity, $\mathbf{L}_e \in \mathbb{R}^T$, and heat, $\mathbf{L}_h \in \mathbb{R}^T$, demand profiles. Data are available at every hour of the year.
iv. The set of available technologies with the corresponding performance and cost coefficients.

2.2. Decision variables

The following decision variables are returned:

i. The size of the installed technologies, $\mathbf{S} \in \mathbb{R}^M$ (deciding $\mathbf{S}$ also implies selecting the technologies).
ii. The on/off status, $\mathbf{x} \in \{0,1\}^{M_A\times T}$, of those M_A conversion technologies which must be described accordingly.
iii. The input power, $\mathbf{F} \in \mathbb{R}^{M\times T}$, and output power, $\mathbf{P} \in \mathbb{R}^{M\times T}$, of the conversion and storage technologies.
iv. The stored energy, $\mathbf{E} \in \mathbb{R}^{M_s\times T}$, of the storage technologies M_s.
v. The imported electrical and gas power, $\mathbf{U}_e$ and $\mathbf{U}_g \in \mathbb{R}^T$, respectively, and the exported electrical power, $\mathbf{V}_e \in \mathbb{R}^{M\times T}$. Note that the exported electrical power must be determined separately for each technology due to the different selling prices.

While the size and selection of the installed technologies is typically referred to as a design variable, decision variables (ii)–(v) are denoted as operation variables and are determined at every hour of the year.

2.3. Constraints

The constraints of the optimization problem can be divided into two categories: (i) performance of the conversion and storage technologies, and (ii) MES energy balances. Both are described in detail in the following.

Performance of conversion and storage technologies. The set of available technologies is indicated with $\mathscr{M}$ and includes all the technologies described below. Here, affine and piecewise affine (PWA) correlations describing the performance of the considered technologies are derived based either on first-principle models or on manufacturer data. In particular, the approach proposed by Yokoyama et al. [33] is used to linearize the power and size dependency of conversion performance. In the following equations, S refers to the size of the technology of interest, i.e. the rated input power. For each technology $i \in \mathscr{M}$, S_i must vary between a minimum and a maximum value, $S_i^{\min}$ and $S_i^{\max}$ respectively:

$$S_i^{\min} a_i \leqslant S_i \leqslant S_i^{\max} a_i \tag{2}$$

where the binary variable $a_i \in \{0,1\}$ indicates whether the i-th technologies is installed. The following constraints hold for all time steps $t \in \{1,...,T\}$ (the linear coefficients for all the investigated technologies are reported in Table 1):

- Photovoltaic (PV) panels, generating electricity from solar energy: the generated electrical power P_t is expressed as

$$P_t < \eta(I_t,\Theta_t) I_t S \tag{3}$$

where S is the installed PV area, limited by the roof area availability; η is the pre-determined conversion efficiency, modeled as a function of air temperature Θ_t and solar radiation I_t, based on the approach suggested by De Soto et al. [34]: an average value around 0.15 is obtained for our case using that approach. Note that P_t is the t-th element of the vector $\mathbf{P}$ (similar notation is used for all the other vectors).
- Thermal solar (TS) panels, generating heat from solar energy: the generated thermal power P_t is expressed as

$$P_t = \eta I_t S \tag{4}$$

where S is the installed TS area, limited by the roof area availability;

Table 1
Input data for description of conversion and storage technologies.

Conversion technology	α	β	γ [kW]	δ	ζ [kW]	κ	ν [kW]	ρ
edHP	3.59	−0.08	0.10	0.13	0.01	0.99	0.01	
MGT	{0.36, 0.33}	{−0.02, 0.00}	{−6.72; −7.02}	{0.17; 0.00}	{−0.58; 108}	{1; 1}	{0; 0}	3.01
Boiler [39]	0.92	0	0	0	0	0	0	
NG SOFC	{0.71, 0.61, 0.51, 0.41}	{−0.05, −0.02, 0.04, 0.11}	0	0.14	0	1	0	1.46
NG PEMFC	{0.54, 0.47, 0.41, 0.36}	{−0.04, −0.01, 0.02, 0.06}	0	0.19	0	1	0	2.01
PtG								
H_2-air PEMFC	{0.59, 0.54, 0.50, 0.47}	{−0.00, 0.02, 0.06, 0.11}	0	0.01	0	1	0	1.71
PEME	{0.60, 0.55, 0.53, 0.51}	{−0.01, 0.020, 0.01, 0.03}	0	0.07	0	1	0	

Storage technology	η	Λ [h^{-1}]	Π	τ [hr]	$\Theta^{\min}$ [°C]	$\Theta^{\max}$ [°C]	p[bar]
LiB [40]	0.96	0.001	0	3			
HS [41]	1	0	0	4			40
HWTS [42]	0.95	0.005	0.001	4	65	90	1.01

η is the conversion efficiency, which is typically given as function of the generated heat temperature: here it is assumed to be constant, and equal to 0.65 [35]. Note that the sum of installed PV and TS area is also limited by the total availability.

- Electricity-driven heat pumps (edHPs), generating heat by absorbing electricity: given the Swiss boundary conditions, here the heat pumps are only used to provide heat. The generated thermal power is expressed as

$$P_t = \alpha F_t f(\Theta_t) + \beta S x_t + \gamma x_t \tag{5}$$

where

$$x_t(\delta S + \zeta) \leqslant F_t \leqslant x_t(\kappa S + \nu) \tag{6}$$

Here x_t is a binary variable indicating whether the device is turned on at time step t, producing power but also incurring in a minimum power consumption $\delta S + \zeta$; the parameters $\alpha,\beta,\gamma,\delta,\zeta,\kappa,\nu$ linearly correlate the generated power P_t to the input power F_t and the unit size S, and are determined by fitting manufacturer data for several sizes and part-load conditions [36]; the influence of air temperature on the efficiency is taken into account through the given function $f(\Theta_t)$, based on the data presented in [37]. Finally, note that the bilinearity Sx_t between a continuous and a binary variable can be formulated as a linear constraint through the introduction of an auxiliary variable $\widetilde{S_t} = Sx_t$ [38]:

$$S^{\min} x_t \leqslant \widetilde{S_t} \leqslant S^{\max} x_t \tag{7}$$

$$S - S^{\max}(1 - x_t) \leqslant \widetilde{S_t} \leqslant S \tag{8}$$

- Micro-gas turbines (MGTs) generating electricity and heat from natural gas (NG): the generated electrical power is expressed as

$$P_t = (\boldsymbol{\alpha}\cdot\mathbf{b})F_t + (\boldsymbol{\beta}\cdot\mathbf{b})Sx_t + (\boldsymbol{\gamma}\cdot\mathbf{b})x_t \tag{9}$$

where

$$(\boldsymbol{\delta}\cdot\mathbf{b})Sx_t + (\boldsymbol{\zeta}\cdot\mathbf{b})x_t \leqslant F_t \leqslant (\boldsymbol{\kappa}\cdot\mathbf{b})Sx_t + (\boldsymbol{\nu}\cdot\mathbf{b})x_t \tag{10}$$

$$\mathbf{b}\cdot\mathbf{1} \leqslant 1 \tag{11}$$

$$b_1 S^{\min} + b_2 S^{\text{int}} \leqslant S \leqslant b_1 S^{\text{int}} + b_2 S^{\max} \tag{12}$$

Here two different sets of linear coefficients α - ν are implemented to distinguish between devices below and above a certain size S^{int}. In other words, different affine approximations are implemented for different size ranges, which are identified through the binary variable $\mathbf{b} \in \{0,1\}^2$. This allows a better fitting of manufacturer data [43].

Micro gas turbines produce at the same time electrical and thermal power Q_t, the two being related by

$$Q_t = P_t(\rho - 1) \tag{13}$$

where ρ is the average ratio of first-principle efficiency to electrical efficiency.

- Fuel cells and electrolyzers: both solid oxide fuel cells (SOFCs) and proton exchange membrane fuel cells (PEMFCs) are considered. While SOFC run on NG, PEMFC can use NG or hydrogen (H_2) as fuel. A proton exchange membrane (PEM) electrolyzer is also included, generating hydrogen and oxygen by absorbing electrical power. The produced hydrogen and oxygen can be stored in pressurized tanks. The possibility of producing and re-converting hydrogen is here referred to as power-to-gas (PtG). For the fuel cell, P_t and F_t refer to generated electrical power and inlet fuel power (fuel LHV), respectively. For the electrolyzer P_t and F_t refer to generated fuel power (hydrogen LHV) and absorbed electrical power, respectively.

For both devices, a piecewise affine approximation based on first-principle models is implemented to describe the conversion efficiency, as discussed in [44,45]. For all line segments $i = \{1,\ldots,m\}$:

$$P_t \leqslant \alpha_i F_t + \beta_i S x_t \tag{14}$$

where

$$\delta S x_t \leqslant F_t \leqslant S x_t \tag{15}$$

Here the parameters α_i and β_i are the coefficients of the i-th approximating line segment. Note that due to the modularity of these systems the size does not significantly affect the performance, translating into $\gamma = \zeta = \nu = 0$.

Like MGTs, fuel cells produce at the same time electrical and thermal power Q_t, the two being related by Eq. (13). Note that start-up/shut-down and ramp-up/ramp-down limitations of fuel cells, electrolyzers and micro gas turbines are modeled through the set of linear constraints presented by Arroyo and Conejo in [46] (in particular, we refer to Eqs. (1)–(12) in that paper), where two additional binary variables y_t and z_t are introduced.

An additional remark about the oxidant fed to the fuel cells (FCs) is worth making. In this work, oxygen from air is used instead of pure oxygen produced by the electrolyzer. Although this translates into a lower electrical efficiency of the fuel cell, it avoids: (i) the oversizing of electrolyzer and storage tanks (oxygen is produced by the PEM electrolyzer with a H_2:O_2 ratio of 2:1 and consumed by the PEM fuel cell with a H_2:O_2 ratio of 1.15:1), (ii) the injection of excess hydrogen into the natural gas grid, which is still a debated procedure in terms of cost and flow rate limitations.

- Boiler, generating heat from natural gas: the generated thermal power is expressed as

$$P_t = \alpha F_t \tag{16}$$

where

$$0 \leqslant F_t \leqslant S \tag{17}$$

Here, the size dependency of boiler performance is neglected, and no minimum value is imposed for the generated power. A conservative treatment is adopted, as the boiler is used as a reference technology for thermal generation.

- Storage systems: three types of storage systems are considered: (i) hot water sensible thermal storage (HWTS), (ii) lithium battery (LiB), and (iii) H_2 tank storage (HS). Although latent and thermochemical thermal storage systems promise to be suitable solutions for long-term storage in the near future [47], sensible thermal storage represents the cheapest, most developed and commercial system. In this work, HWTS is considered, where the water is stored at 90 °C and cooled to 65 °C. Due to the fairly high energy losses and the low energy density, this system is mainly used to overcome short-term mismatch between thermal energy generation and use. Similarly, battery storage is mainly used for short-term electricity compensation due to its energy losses and high investment cost. On the contrary, H_2 storage features negligible energy losses, and therefore represents a promising solution for offsetting seasonal mismatch between renewable energy generation and energy consumption. The HS is coupled with the PtG system to generate, store and use hydrogen. In this context, hydrogen can be generated at high pressure, 40 bar here. While on the one hand HS has very limited energy losses in time, on the other hand the round-trip efficiency of the overall PtG process is around 40%, much lower than that of thermal and battery storage systems (see Table 1). For this reason, HS represents an efficient alternative when storing energy for long time periods. It is worth mentioning that the different utilization of the storage units typically translates into a larger installed size for the HS than for HWTS and LiB.

All the aforementioned storage units are described through the following linear equations:

$$E_t = E_{t-1}(1-\Lambda\Delta t) - (\Pi Sg(\Theta_t) + \eta P_t)\Delta t \tag{18}$$

where

$$E_0 = E_T \tag{19}$$

$$g = \frac{\Theta^{\min} - \Theta_t}{\Theta^{\max} - \Theta^{\min}} \tag{20}$$

$$0 \leqslant E_t \leqslant S \tag{21}$$

$$-\frac{S}{\tau} \leqslant P_t \leqslant \frac{S}{\tau} \tag{22}$$

Here P_t assumes positive or negative values for charging and discharging power, respectively; Λ and Π are self-discharge parameters, and $g(\Theta_t)$ expresses the influence of the ambient temperature on the losses of the storage devices, as suggested in [23] for the thermal storage; η indicates the charging/discharging efficiency; Δt is the duration of the time interval t; τ is the time required to fully charge or discharge the storage. Note that the same value for charging and discharging efficiency is assumed. As the two efficiencies are typically similar, there is no need for binary variables specifying whether the device is charging or discharging. The periodicity constraint, Eq. (19), imposes the same storage level at the beginning and at the end of the year.

Note that in the present form the optimization framework does not include considerations on possible malfunction of the devices.

MES energy balances. The set of considered energy carriers within the multi-energy system is indicated with $\mathscr{N}$ and includes:

- Electricity (e): it can be consumed and generated by the conversion technologies, stored by the storage units, exchanged with the electrical grid and utilized by the end users.
- Heat (h): it can be generated by the conversion technologies, stored by the storage units and utilized by the end users.
- Natural gas (g): it can be imported from the gas grid and consumed by the conversion technologies.
- Hydrogen (H_2): it can be consumed and generated by the conversion technologies, stored by the storage units, and injected into the gas grid.

It is worth noting that cooling is not considered here; however, it could easily be included.

The sum of imported and generated power must equal the sum of exported and used power for each energy carrier $j \in \mathscr{N}$ for all time steps $t \in \{1,...,T\}$. This can be expressed in general form as

$$\sum_{i \in \mathscr{M}} (U_{j,i,t} + P_{j,i,t} - V_{j,i,t} - F_{j,i,t}) - L_{j,t} = 0 \tag{23}$$

Here, U is the imported energy, P the generated energy, V the exported energy, F the absorbed energy and L the energy required by the end users. With this notation, the set of technologies $\mathscr{M}$ also includes the direct utilization of the energy carriers. Note that limitations on the imported and exported energy could easily be included if necessary.

An additional remark about the modeling of electricity and heating demands is needed. These demands are modeled for several buildings based on a neighborhood in Zurich, Switzerland, following the approach presented in [48]. A centralized energy hub is assumed to be located at the center of the neighborhood, and an approximate grid topology for the district heating is considered using a shortest path algorithm. Based on the calculated distance between the hub and the buildings, the original heat demand of each building is updated to account for transport losses. A specific heat demand increment of 4% per km is assumed [49]. Also, an auxiliary electricity consumption of 8.5% of the heat demand is considered for pumping [15]. Finally, the electricity and heat demands for all buildings are aggregated and the total demands are implemented.

2.4. Objective function

The objective function of the optimization problem is the total annual cost of the system, J, given by the sum of three contributions, namely the capital, J_c, operation, J_o, and maintenance, J_m, annual costs.

The annual capital cost is expressed as

$$J_c = \sum_{i \in \mathscr{M}} (\lambda_i S_i + \mu_i)\omega_i \tag{24}$$

where λ_i and μ_i represent the variable and fixed cost coefficients for the i-th technology; S_i indicates the unit size, i.e. the rated input power for non-solar conversion technologies, the rated stored energy for storage technologies, and the installed area for solar panels. To compute the equivalent annual investment cost, the annuity factor ω is included, which is calculated using the standard definition and based on an interest rate of 6%. A piecewise affine approximation is implemented to model the size dependency of the capital cost. For each technology $i \in \mathscr{M}$:

$$\lambda_i = \mathbf{w}_i \cdot \boldsymbol{\theta}_i,\ \mu_i = \mathbf{w}_i \cdot \boldsymbol{\pi}_i,\ \mathbf{w}_i \cdot \mathbf{1} \leqslant 1 \tag{25}$$

$$\mathbf{w}_i \cdot \mathbf{S}_i^{\min} \leqslant S_i \leqslant \mathbf{w}_i \cdot \mathbf{S}_i^{\max} \tag{26}$$

where $\mathbf{w}_i \in \{0,1\}^m$ is a binary variable specifying the active line segment for the capital cost calculation of technology i, where m is the number of line segments; $\boldsymbol{\theta}_i, \boldsymbol{\pi}_i \in \mathbb{R}^m$ are the variable and fixed costs of a specific line segment, respectively; $\mathbf{S}_i^{\min}, \mathbf{S}_i^{\max} \in \mathbb{R}^m$ are the minimum and maximum size values of every line segment, respectively. Since the capital cost must be minimized, and due to the concavity of the curve, a binary variable for each line segment is required to identify the active linear approximation. The cost approximation for two exemplary technologies, namely heat pump and thermal storage, is illustrated in Fig. 2. Table 2 reports the cost coefficients for all the investigated conversion and storage technologies, as well as their capacity constraints.

The annual operation cost is calculated based on the amount of imported and exported electricity and gas during the year:

$$J_o = \sum_{j \in \mathscr{N}} \sum_{i \in \mathscr{M}} \sum_{t=1}^{T} (u_{j,t} U_{j,i,t} - v_{j,i,t} V_{j,i,t})\Delta t \tag{27}$$

where import and export prices, u and v, and powers, U and V, depend

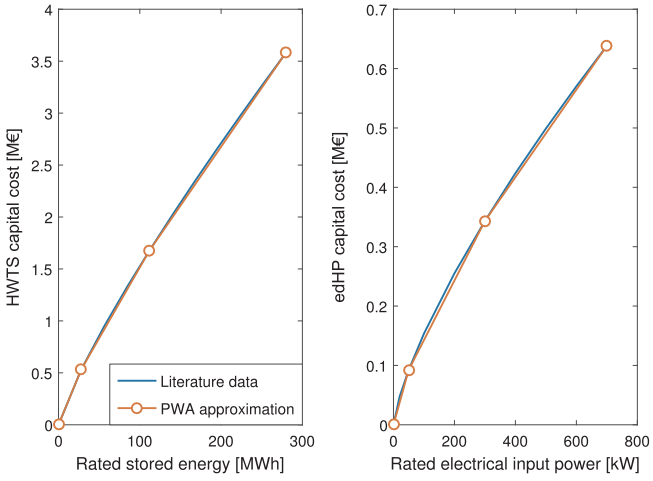

Fig. 2. PWA approximation for the calculation of the capital cost of heat pump (edHP) and hot water thermal storage (HWTS).

Table 2
Cost coefficients of conversion and storage technologies.

Technology	θ	μ [€]	S^{min}	S^{max}	ψ
PV [50]	300 €/m^2	0	0 m^2	6000 m^2	0.05
TS [50]	500 €/m^2	0	0 m^2	6000 m^2	0.03
edHP [51,52]	{2088;1221;930.9} €/kW	{0;4.33;13.0} × 10^4	{0;50;300} kW	{50;300;700} kW	0.015
MGT [43]	{738.4;892.5;716.1} €/kW	{4.38;0.93;33.0} × 10^4	{112;224;1818} kW	{224;1818;3030} kW	0.05
boiler [39]	{194.1;82.4;65.2} €/kW	{0;6.88;10.4} × 10^3	{0;70;200} kW	{70;200;2500} kW	0.02
NG SOFC [53]	{4260;2580;1320} €/kW	{0;1.12;2.80} × 10^6	{0;800;1600} kW	{800;1600;2500} kW	0.08
NG PEMFC [53]	{2320;1360;640} €/kW	{0;9.60;2.40} × 10^5	{0;800;1600} kW	{800;1600;2500} kW	0.08
H_2 PEMFC [53]	{2160;1680;1320} €/kW	{0;3.20;8.00} × 10^5	{0;800;1600} kW	{800;1600;2000} kW	0.08
PEMEC [53]	{2693;1727;1354} €/kW	{0;9.67;2.46} × 10^4	{0;200;800} kW	{200;800;2000} kW	0.05
LiB [54]	500 €/kWh	0	0 kWh	10000 kWh	0.020
HS [55]	{20.7;13.6;10.9} €/kWh	{0;2.35;94.5} × 10^3	{0;0.05;5.55} × 10^3 kWh	{0.05;5.55;150} × 10^3 kWh	0.03
HWTS [42]	{10.5;7.5;6.25} €/kW	{0;8.4;22.9} × 10^4	{0;0.28;11.4} × 10^4 kWh	{0.28;11.4;28.0}·10^4 kWh	0.02

on the energy carrier j, technology i, design day d and time instant t. A feed-in-tariff strategy is considered for the electricity sold by PV panels, i.e. $v_{e,PV,t} = 0.15$ €/kWh $\forall\, t$, while a lower electricity selling price, 0.05 €/kWh, is assumed for the other conversion and storage technologies. The Swiss electricity spot market price for 2016, which varies from 0.01 to 0.12 €/kWh is used [56], whilst a constant import price of 0.064 €/kWh is used for natural gas [57].

The annual maintenance cost is given as a fraction ψ of the annual capital cost [52,53]:

$$J_m = \sum_{i \in \mathcal{M}} \psi_i J_{c,i} \tag{28}$$

Along with the total annual cost, the system is also evaluated in terms of environmental performance by means of the ε-constraint method. This translates into a minimum-cost optimization problem, where the annual CO_2 emissions are constrained below a maximum threshold. The total annual emission is calculated as the sum of the contributions of electricity and gas imported from the grid:

$$e = \sum_{j \in \mathcal{N}} \varepsilon_j \left(\sum_{i \in \mathcal{M}} \sum_{t=1}^{T} U_{j,i,t} \Delta t \right) \tag{29}$$

where ε_j is the specific carbon dioxide emission of carrier j, assumed to be constant along the year. The values of the emission coefficients for electricity and gas are $\varepsilon_e = 0.137$ ton_{CO_2}/MWh and $\varepsilon_g = 0.237$ ton_{CO_2}/MWh, respectively. Note that the Swiss energy mix strongly relies on hydroelectric and nuclear power, thus resulting into low CO_2 emissions for grid electricity.

2.5. Time horizon modeling

So far, we have described the optimization problem considering as time horizon one year with hour resolution, i.e. $T = 8760$. Because of the large number of variables and constraints arising when investigating different technology options, the full scale optimization is hardly feasible and the time variability during the year is normally simplified. Recently, Pfenninger presented a systematic analysis of the different techniques to reduce the time resolution of energy models [58], including time slices and representative design days or weeks. Here, a set of D design days and their sequence σ along the year are identified by using the MATLAB®-embedded clustering algorithm k-means [59]. Based on weather conditions, energy prices and load profiles (i.e. input data (i)–(iii)), the algorithm solves a mixed-integer nonlinear problem to identify the most representative set of D design days and to assign every day of the year to a specific design day $d \in \{1,...,D\}$, characterized by its own typical hour resolution. The original formulation of k-means clustering, or Lloyd's algorithm, was presented by Lloyd in [60]. It is worth mentioning that the clustering procedure would level off the original input profiles, reducing the variation between the minimum and maximum values. Consequently, a system design based on such clustered input profiles would not be able to meet the energy demand at every hour of the year. To address this issue, and having in mind that the primary goal of the hub is to satisfy the user demand, the clustering procedure has been constrained to maintain the minimum and maximum values of the original demand profiles.

The traditional MILP formulations based on design days are not able to include seasonal storage. In the following, three methods for modeling the time horizon are discussed: M0, which is the existing method that excludes seasonal storage, and M1 and M2, which are proposed in this work as alternative solutions that allow including seasonal storage.

Method 0 (M0) – Traditional approach. The traditional approach, hereafter denoted as method 0 (M0), considers uncoupled design days: The sequence of design days along the year is not considered in the optimization problem, which is therefore formulated independently for each design day d. As an example, the equations describing the power generated by fuel cell and electrolyzer devices (Eqs. 14,15) are recast as:

$$P_{d,k} \leqslant \alpha_i F_{d,k} + \beta_i S x_{d,k} \tag{30}$$

$$\delta S x_{d,k} \leqslant F_{d,k} \leqslant S x_{d,k} \tag{31}$$

where $d \in \{1,...,D\}$ indicates the d-th design day and $k \in \{1,...,K\}$ the k-th daily time instant, with hour resolution hence $K = 24$. Similarly, the storage dynamics (Eqs. (18) and (19)) becomes

$$E_{d,k} = E_{d,k-1}(1-\Lambda\Delta k) - \Pi Sg(\Theta_{d,k})\Delta k + \eta P_{d,k}\Delta k\ ,\ \forall\ d,k \tag{32}$$

$$E_{d,0} = E_{d,T}\ ,\ \forall\ d \tag{33}$$

where the periodicity constraint, Eq. (33), is written independently for each d-th design day, thus decoupling each day from both the previous and the next. Note that this may result into a mismatch between the energy stored at the end of a day and the energy stored at the beginning of the following one. Following the same logic, the energy balances of Eq. (23) are recast as:

$$\sum_{i \in \mathcal{M}} (U_{j,i,d,k} + P_{j,i,d,k} - V_{j,i,d,k} - F_{j,i,d,k}) - L_{j,d,k} = 0\ ,\ \forall\ j,d,k \tag{34}$$

and the annual operation cost of Eq. (27) is given by

$$J_o = \sum_{j \in \mathcal{N}} \sum_{i \in \mathcal{M}} \sum_{d=1}^{D} \Gamma_d \left[\sum_{k=1}^{K} (u_{j,d,k} U_{j,i,d,k} - v_{j,i,d,k} V_{j,i,d,k}) \Delta k \right] \tag{35}$$

where Γ_d is the number of design days of type d occurring during the year (hence $\sum_{d=1}^{D} \Gamma_d = 365$).

Although this approach reduces the complexity of the optimization problem, as D is smaller than 365, the discontinuity between different design days does not allow to describe seasonal operating cycles,

therefore resulting in a daily operation of the multi-energy system. In the following, two novel approaches are proposed to allow for long-term system operation while at the same time limiting the computational complexity of the optimization problem.

Method 1 (M1) – Coupling design days. The first approach proposed in this paper, hereafter named method 1 (M1), allows for the optimization of the level of stored energy hour-by-hour while still describing the year time variability through typical design days. This requires the introduction of the sequence σ of design days, which allows to couple successive days of the year. In other words, the energy stored during the last hour of every day of the year is connected to the energy stored during the first hour of the following day, where each day of the year is described by a given design day. Note that σ takes each day of the year y and returns the corresponding design day d, i.e. $1 \leqslant y \leqslant 365, 1 \leqslant \sigma(y) \leqslant D$. In this case, the storage dynamics of Eqs. (32) and (33) is written as:

$$E_{y,k} = E_{y,k-1}(1-\Lambda\Delta k)-\Pi Sg(\Theta_{y,k})\Delta k + \eta P_{\sigma(y),k}\Delta k \ , \forall\ y \ ,\forall\ k \in \{2,...,K\} \tag{36}$$

$$E_{y,1} = E_{y-1,K}(1-\Lambda\Delta k)-\Pi Sg(\Theta_{y,1})\Delta k + \eta P_{\sigma(y),1}\Delta k \ , \forall\ y \tag{37}$$

$$E_0 = E_{Y,K} \tag{38}$$

where $y \in \{1,...,Y\}$ indicates the y-th day of the year, with $Y = 365$; $P_{\sigma(y),k}$ is the charging/discharging power at day y, described by the typical day $\sigma(y)$. Eqs. (36)–(38) imply that, although two days of the year described by the same design day must be characterized by the same variation in stored energy, they can have different values of stored energy at the beginning of each day. The improved storage flexibility obtained with respect to M0 comes at the price of a larger number of variables and constraints. Indeed, $\mathbf{E} \in \mathbb{R}^{Y\times K}$ (instead of $\mathbf{E} \in \mathbb{R}^{D\times K}$) can now assume different values at every hour of the year, and the corresponding number of constraints is imposed by Eqs. (36) and (37). As for the full scale optimization, the periodicity constraint, Eq. (38), is imposed on the whole year, instead of on each design day.

Method 2 (M2) – Detailed input data. The second approach proposed, hereafter named method 2 (M2), allows to optimize the storage operation hour-by-hour while considering the actual energy demands. The underlying consideration is that the computational complexity of the optimization problem is mainly caused by binary variables. Thus, the method divides the aforementioned operation variables (i.e. decision variables (ii)–(v)) in two categories: (A) operation variables related to binary variables, and (B) other operation variables not related to binary variables. Group A includes the operation variables of those technologies characterized by an on/off status, i.e. the on/off status and the input/output power of heat pump, micro gas turbine, fuel cells and electrolyzer (subset $\mathscr{M}_A$). Since such variables represent the main source of computational complexity, their number is limited by using typical design days. Group B includes all other decision variables, namely the imported/exported grid energy, the charging/discharging energy and the stored energy, and the power generated by those conversion technologies where the on/off status is neglected, i.e. renewable-based technologies and boiler (subset $\mathscr{M}_B$). These variables are defined at every hour of the year.

This classification of the decision variables affect the formulation of both constraints and objective function. In particular, as group A is modeled using design days (e.g. Eqs. (30) and (31)) and group B using every hour of the year (e.g. Eqs. (18)–(22)), the sequence of design days σ couples the two types of decision variables within the energy balances and the objective function (following the same logic of Eq. (36)). The energy balances, Eq. (23), become:

$$\sum_{i\in\mathscr{M}_A}(U^A_{j,i,\sigma(y),k} + P^A_{j,i,\sigma(y),k} - V^A_{j,i,\sigma(y),k} - F^A_{j,i,\sigma(y),k}) + + \sum_{i\in\mathscr{M}_B}(U^B_{j,i,y,k} + P^B_{j,i,y,k} - V^B_{j,i,y,k} - F^B_{j,i,y,k}) - L_{j,y,k} = 0 \ , \forall\ j,y,k \tag{39}$$

Similarly, the annual operation cost, Eq. (27), becomes

$$J_o = \sum_{j\in\mathscr{N}}\sum_{i\in\mathscr{M}_A}\sum_{d=1}^{D}\Gamma_d\left[\sum_{k=1}^{K}(u^A_{j,\sigma(y),k}U^A_{j,i,\sigma(y),k} - v^A_{j,i,\sigma(y),k}V^A_{j,i,\sigma(y),k})\Delta k\right] + + \sum_{j\in\mathscr{N}}\sum_{i\in\mathscr{M}_B}\sum_{y=1}^{Y}\sum_{k=1}^{K}(u^B_{j,i,y,k}U^B_{j,i,y,k} - v^B_{j,i,y,k}V^B_{j,i,y,k})\Delta k \ , \forall\ y,k. \tag{40}$$

This method features a higher flexibility for the multi-energy system compared to the previous approaches, which comes at the cost of a

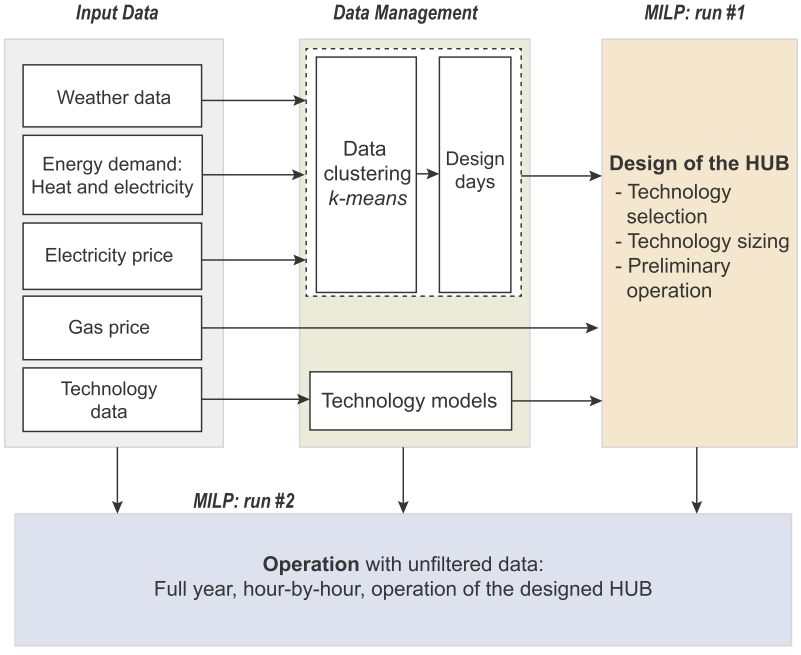

Fig. 3. Optimization framework implemented to perform and evaluate the design of multi-energy systems.

higher number of decision variables and constraints. Finally, note that for both M1 and M2 σ enables the coupling of the dynamics of conversion technologies of group A during two successive days of the year.

The overall optimization framework considered in this work is summarized in Fig. 3. First, the set of typical design days is determined as described above. Based on the adoption of such design days, the optimal design of the multi-energy system is carried out, i.e. technology selection, sizing and operation. Afterward, with the aim of assessing the quality of the different methods, the system design is tested by running the operation with the real hour-by-hour input data, i.e. no design days are used and the system topology is fixed by the design procedure.

3. Results

In this section, first, the validity of the proposed techniques is tested by considering a simple multi-energy system that can be solved in a reasonable computational time without resorting to design days. Next, the developed tool is applied to minimize the total annual cost and emissions of a multi-energy system characterized by a wider park of conversion and storage technologies.

3.1. Comparison of M0, M1 and M2 for a simple MES

The set of available technologies considered in this simplified case is reported on the left-hand side of Fig. 4, which also shows the selected configuration on the right-hand side. The system can include PV panels, boiler, battery and PtG system. The PtG system consists of a PEM electrolyzer (PEME) and a PEM fuel cell using H_2 and air to generate electricity and heat; moreover, it is coupled with a hydrogen tank (HS), which ensures the possibility of seasonal storage. The optimization problem is formulated as a single-objective MILP that minimizes the total annual cost of the system, with no additional constraints on the CO_2 emissions. In this context, a maximum size of 1 MW is imposed for the boiler to ensure the operation of the PtG, which would not be convenient otherwise. Here, the new methods, M1 and M2, are compared with the traditional approach (M0) and the full scale optimization (FSO). The comparison is performed in terms of computational time, system design, operation and annual costs. The MILP is solved by using the commercial software IBM CPLEX 12.7 [61], set to have a relative MIP gap of 0.01% and an aggressive policy for Gomory fractional cuts and probing.

Fig. 5 shows the size of the HS and the PEME as function of the design days, which vary from a minimum of 3 to a maximum 72. The PV panels and the battery are not selected, whereas the size of the boiler is constant and equal to 1 MW, i.e. the maximum allowed value. It can be noted that, while the traditional approach M0 is unable to exploit a long-term operation of the HS, both M1 and M2 design a storage size similar to FSO. Indeed, the seasonal operation of the storage calls for a larger size of the HS, as this is charged or discharged during periods longer than one day. The figure shows that, independently of the number of design days, M0 provides a HS size much smaller and a PEME much larger than the one obtained with the FSO. In this case, the size of the storage is set by the daily variations in energy demands and prices, whereas the size of the electrolyzer is set by the maximum value of the thermal demand. On the contrary, both M1 and M2 determine a size of the system similar to FSO when implementing a number of typical days above a certain threshold, which is here of about 25 design days. With respect to M1, a better (less conservative) description of the energy demands is obtained when

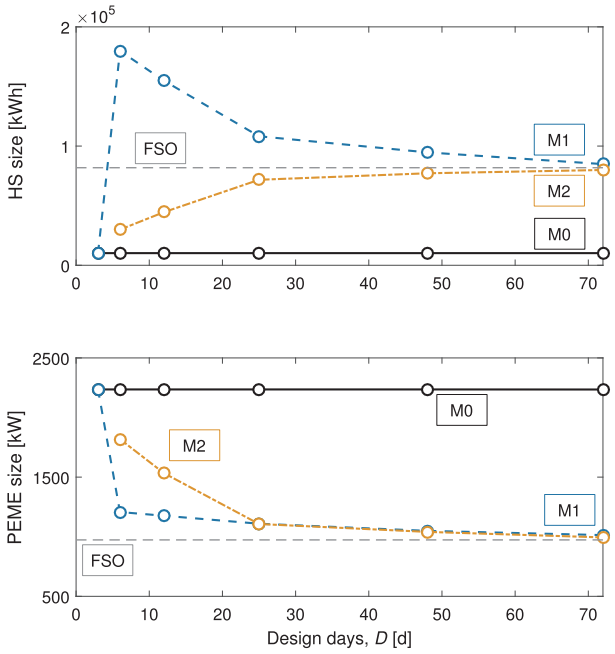

Fig. 5. Size of the hydrogen storage (HS) and PEM electrolyzer (PEME) for M0, M1 and M2 for a number of design days ranging from 3 to 72 and comparison against FSO.

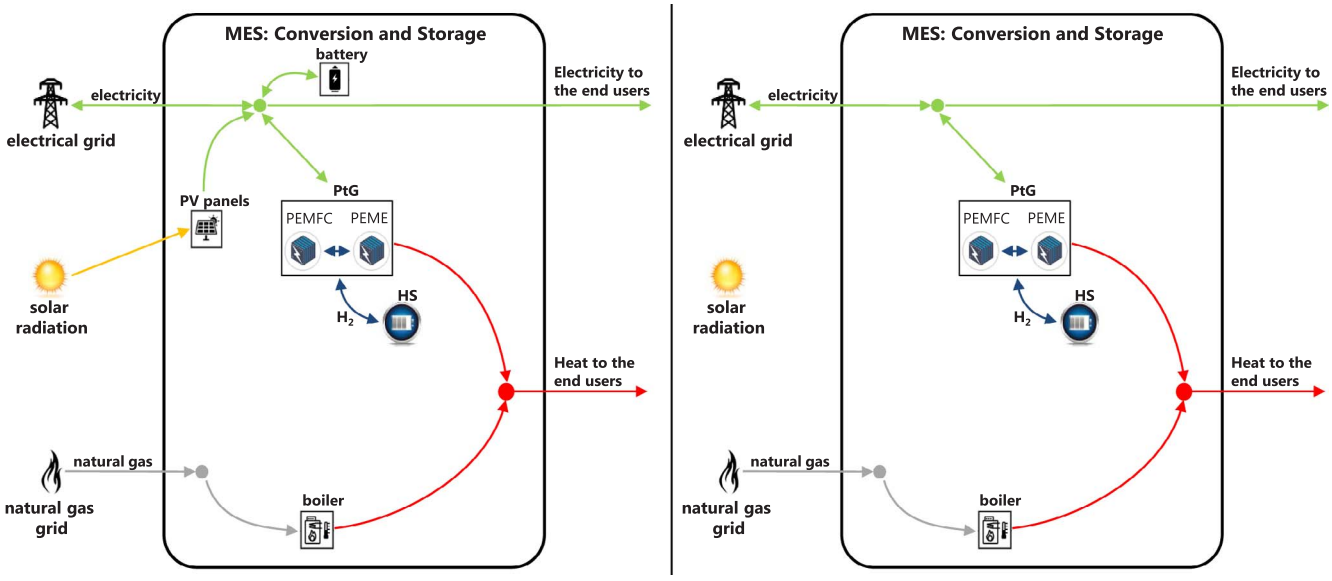

Fig. 4. Schematic representation of the investigated multi-energy system for model validation: set of available technologies (left) and selected configuration (right).

increasing the number of design days, which translates in a more accurate (less conservative) system design. With respect to M2, more design days enable more operation modes of the conversion technologies, which yields a more accurate system operation and design. It is worth noting that M2 is unfeasible when using few typical design days (in this case less than 6), because the produced hydrogen can be reconverted to electricity and heat only according to a limited number of operational modes (i.e. the number of design days), which does not allow to match the thermal supply and demand.

A detailed operation of the HS for M0, M1, M2 and FSO during ten days of the year (10.01–20.01) and as obtained in the design phase with 48 design days, is illustrated in Fig. 6. Notably, M0 results in a daily operation policy, which is different for different design days. On the contrary, M1 and M2 result in a long-term operation policy, similarly to the FSO. In the last four days of the examined period shown in the figure, the storage system is operated following an almost-daily pattern. In this case, all methods behave similarly, as highlighted in the insets at the top-right corner of the figure. Overall, the amount of stored energy along the year is equal to 2.7 GWh for M0, 419 GWh for M1, 386 GWh for M2 and 395 GWh for FSO. This confirms a long-term utilization of the storage system by M1 and M2.

To further test the quality of the different methods, full scale optimizations with unfiltered input data and fixed designs, as described in Fig. 3 are carried out. Results are shown in Fig. 7 in terms of total, capital and operational costs as function of the design days. Again, the full scale optimization can be regarded as benchmark as it achieves the minimum objective function. Notably, the trends of the objective

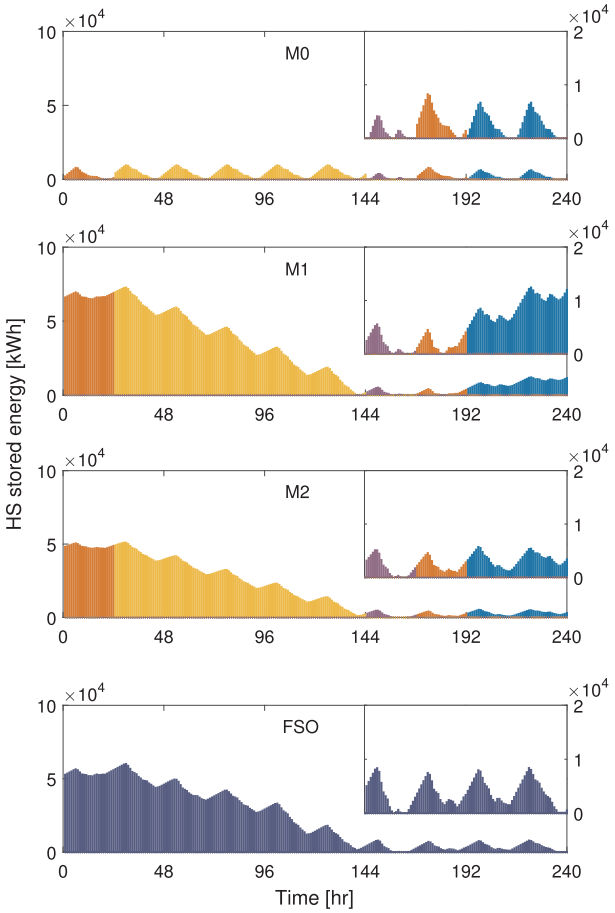

Fig. 6. Optimal operation of the HS along ten days of the year (10.01–20.01) determined by M0, M1, and M2 for 48 design days and comparison against FSO. Same design days are reported with the same colors (red, yellow, purple and blue). (For interpretation of the references to colour in this figure legend, the reader is referred to the web version of this article.)

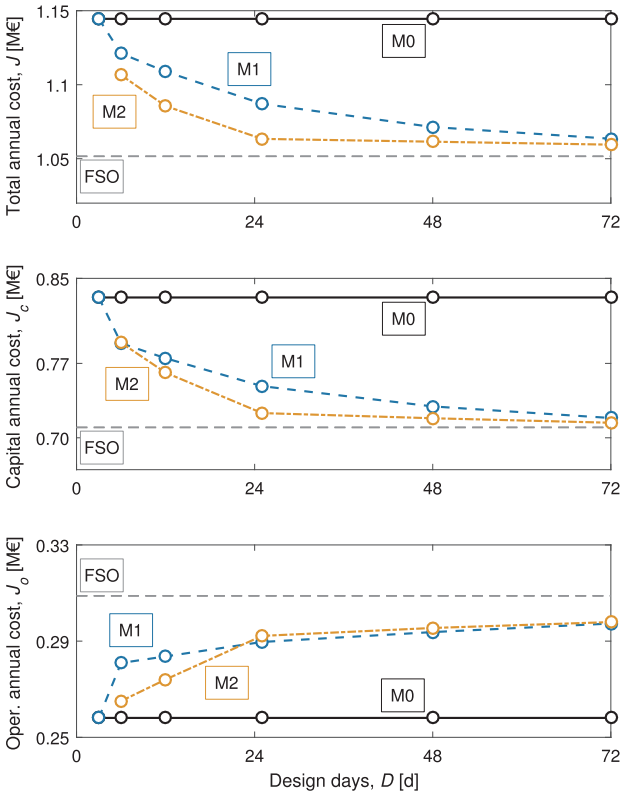

Fig. 7. Total (top), capital (middle) and operation (bottom) annual costs for M0, M1 and M2 for a number of design days ranging from 3 to 72.

function reflect quite well those obtained for the system size: the system design determined by M0, independent of the number of design days, translates into a constant discrepancy in the objective function (around 9% for the total annual cost). On the contrary, a more accurate value of the objective function is determined by M1 and M2 when increasing the number of design days, with the latter approaching faster the value determined by the FSO: a relative error below 1% is obtained by using M2 for a number of design days greater than 24.

Finally, Fig. 8 compares the computation time for the three strategies for a number of typical days ranging from 3 to 72. First, it can be noted that resorting to design days allows to significantly reduce the computation time compared to the FSO, independently of the time horizon description method. Whereas the full scale optimization

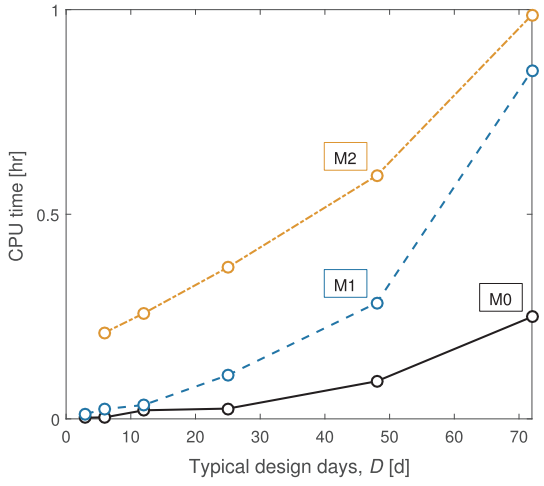

Fig. 8. Computation time of optimization problem for M0, M1 and M2 for a number of design days ranging from 3 to 72. Note that the FSO is not reported here for sake of clarity, as it requires about one day of CPU time.

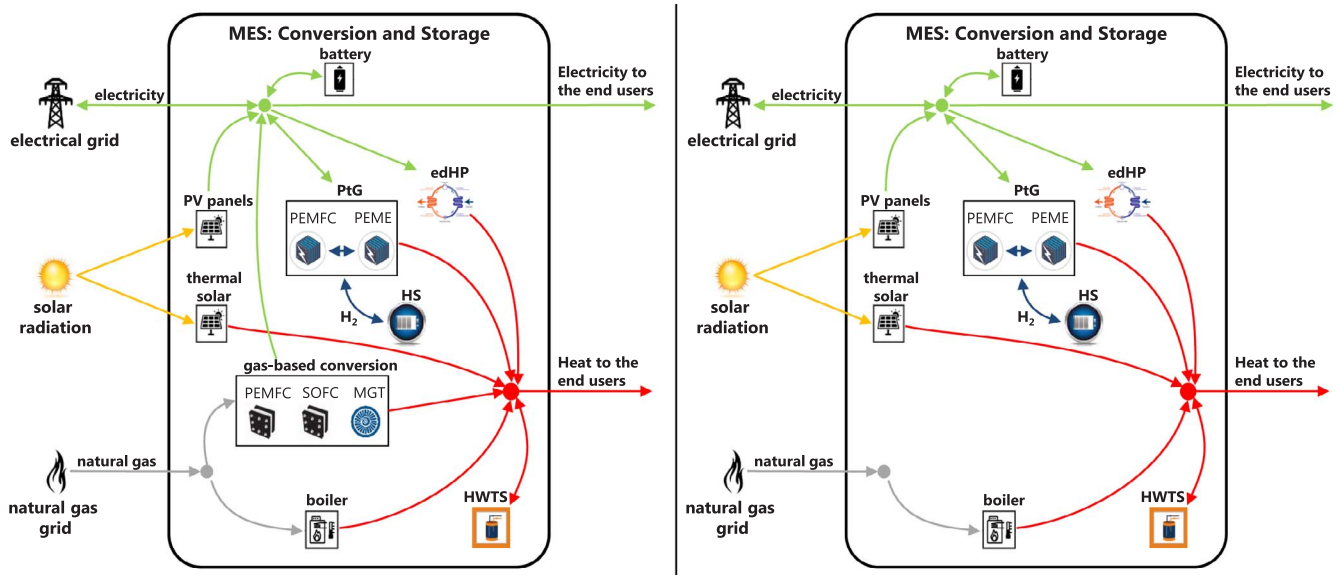

Fig. 9. Schematic representation of the investigated multi-energy system for model application: set of available technologies (left) and selected configuration (right).

requires about 23 h to complete, all the investigated techniques require less than 1 h. Moreover, it can be noted that the additional computation time required by M1 and M2 with respect to M0 is limited. Finally, while M1 has proven to perform generally worse than M2, it however (i) enables the problem resolution with smaller design days and (ii) features a shorter computation time.

3.2. Design of a MES of interest

In the following, we aim at designing a MES starting from a comprehensive set of technologies. To this end, we rely on the use of M2, which proved to be the most accurate approximation of the full scale optimization, when based on 48 design days; this proved to be a reasonable trade-off between results reliability and computation time. No additional constraints on the size of the installed technologies are imposed. In this case, the full scale optimization cannot be completed within five days for a MIP gap of 1%, while the optimization problem is solved within 12 h when implementing M2 with 48 design days. The same solver options described in Section 3.1 are used, but for a MIP gap of 1%. The ε-constraint method is used to minimize both total annual cost and CO_2 emissions of the system: first, two single-objective optimization problems minimizing the total annual cost and the total annual emission of the system are solved, providing the upper and lower limits of annual CO_2 emission, respectively. Next, the emission interval is divided into ten steps and single-objective optimization problems are solved to minimize the total annual cost of the system subject to the corresponding emission constraint. Fig. 9 shows the available technologies on the left-hand side and the selected configuration on the right-hand side: while the system can consist of several conversion and storage technologies, all design points that lay on the cost-CO_2 emission Pareto considers (i) PV and TS panels, (ii) electrical-driven heat pump, (iii) boiler, (iv) battery, (v) sensible thermal storage and (vi) PtG as optimal technologies. These technologies are selected and sized differently for the different Pareto points.

Fig. 10 reports the Pareto front of a reference configuration featuring an available area for solar installation equal to 6000 m^2, which is based on the actual availability of the investigated neighborhood, and highlights the capital and operational cost contributions. It is worth noting that, on the one hand, a more expensive system design is required when reducing the carbon emissions because of the higher capital cost of solar panels and storage systems. Especially, two sharp slope variations, which are due to changes in the hub topology, can be

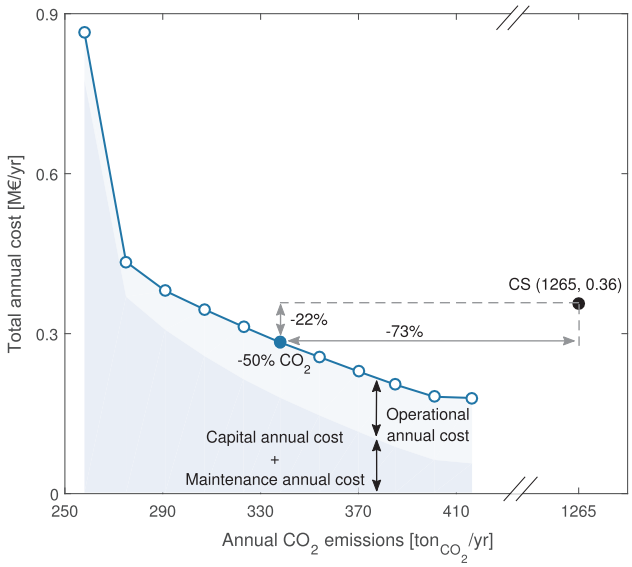

Fig. 10. Cost-emission Pareto front for a reference scenario featuring $A = 6{,}000\ m^2$ of area available for solar installation (M2 with 48 design days). Highlighting of the capital and operation contributions, and comparison with the conventional scenario (CS).

identified when reducing the CO_2 emissions: at about 400 ton_{CO_2}/yr a significant reduction in the boiler size is observed along with a higher utilization of the thermal storage; at about 280 ton_{CO_2}/yr PtG and batteries are added to thermal storage. Before the former, the decrease in CO_2 emissions does not imply a significant increase in cost; after the latter, the decrease in CO_2 emissions comes at a very large increase in the total annual cost. On the other hand, such designs allow to reduce the operation costs substantially, as less natural gas and electricity are imported from the grids.

Moreover, Fig. 10 compares the Pareto set with a conventional scenario (CS) where electricity is bought from the grid and heat is generated using a boiler. Notably, there are design configurations for which a potential reduction in both cost and emissions can be achieved: taking as an example the configuration at 340 ton_{CO_2}/yr (characterized by a 50% emission reduction with respect to the maximum achievable emission reduction), a cost and emission reduction around 22% and 73%, respectively, are achieved with respect to CS.

To investigate the influence of renewables availability on the Pareto

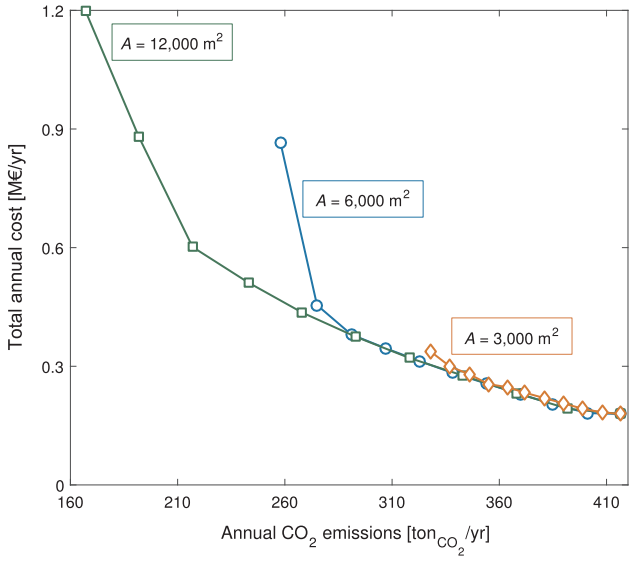

Fig. 11. Cost-emission Pareto fronts for three scenarios characterized by different areas available for solar installation *A*: 3,000 m^2 (red diamond), 6,000 m^2 (blue circle) and 12,000 m^2 (green square). (For interpretation of the references to colour in this figure legend, the reader is referred to the web version of this article.)

front, a sensitivity analysis is performed on the area available for solar installation *A*. Findings are shown in Fig. 11 which presents the Pareto sets for three scenarios characterized by A = 3,000, 6,000 and 12,000 m^2, i.e. half, reference and double available area, respectively. As expected, a higher renewable installation allows to import less energy from the electrical grid and to achieve lower CO_2 emissions. However, in this case larger storage facilities are needed to fully exploit the higher amount of renewable excess generation, thus translating into higher total annual costs at low emission levels (see Fig. 12). Furthermore, it is possible to notice that the three Pareto fronts coincide at high CO_2 emissions, whereas they are separated at low emissions, where the storage technologies play a relevant role.

A better insight on the different hub topologies is illustrated in Fig. 12, which reports the size of the installed technologies as a function of the CO_2 emission reduction. The CO_2 emission reduction is equal to 0 for the minimum cost configuration and 1 for the minimum emission configuration. A few considerations can be made:

i. Natural gas based fuel cells and micro gas turbines, are never installed, independently of the required reduction in CO_2 emissions.
ii. The area available for solar installation determines the minimum carbon emissions that can be reached by the multi-energy system. Independently of its value, the total available area is used uniquely

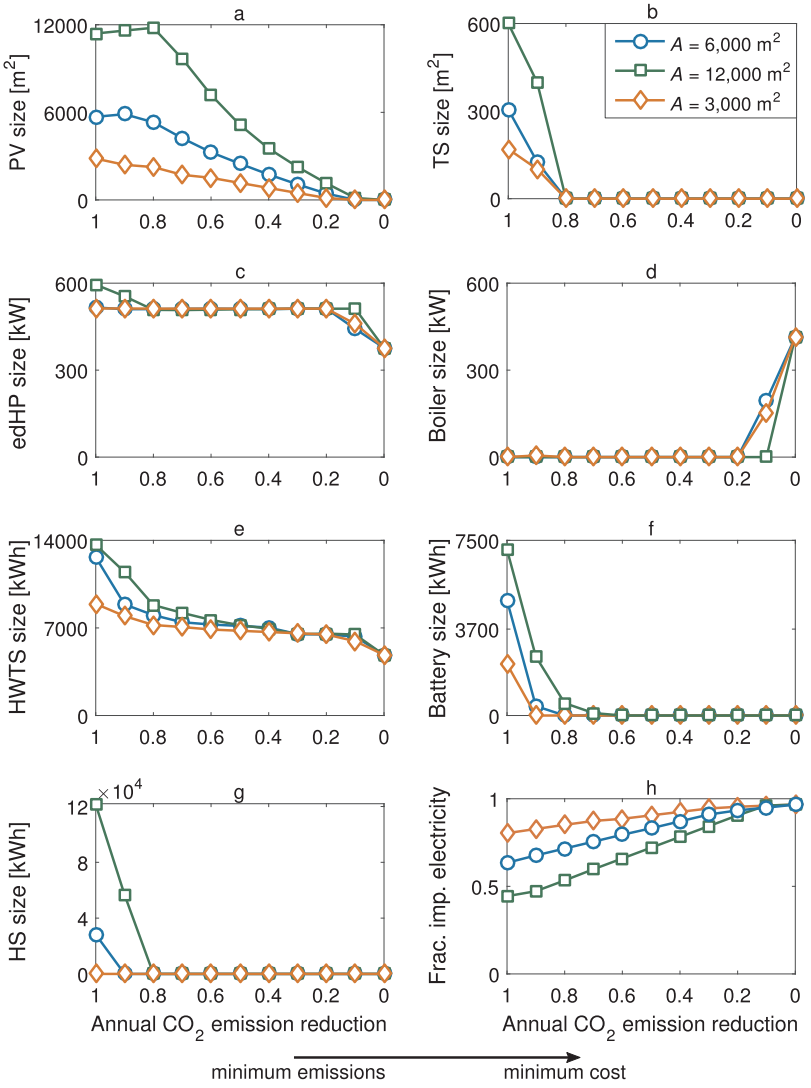

Fig. 12. Size of the installed technologies along the Pareto fronts for 3,000 m^2 (red diamond), 6,000 m^2 (blue circle), 12,000 m^2 (green square): (a) photovoltaic (PV), (b) thermal solar (TS), (c) heat pump (edHP), (d) boiler, (e) battery, (f) sensible thermal storage (HWTS), (g) hydrogen storage (HS). The figure (h) also reports the amount of imported electricity normalized over the whole energy required by the system. (For interpretation of the references to colour in this figure legend, the reader is referred to the web version of this article.)

for PV panels until about a 80% emission reduction, whereas thermal solar panels are installed for a further emission reduction thanks to their higher conversion efficiency (Fig. 12a and b).

iii. Different combinations of boilers and heat pumps are installed along the Pareto fronts to satisfy the thermal demand (Fig. 12c and d), with the former being used only at very low emission reductions (lower than 10–20%). The higher the area available for solar installation, the lower the size of the boiler. Interestingly, a significant heat pump size is always selected despite the high installation cost. This can be explained through an approximate calculation based on average energy prices and conversion efficiencies. Assume the minimum-cost scenario, with no renewable installations. Moreover, assume a cold winter day with conditions favorable to the boiler: average gas price of 0.06 €/kWh, average electricity price of 0.12 €/kWh, average boiler efficiency of 0.92 and average heat pump coefficient of performance of 2.3 (calculated for an ambient temperature of −15 °C). Dividing the average energy prices by the average efficiencies leads to an average thermal energy cost of 0.065 €/kWh for the boiler and of 0.052 €/kWh for the HP. A larger discrepancy is observed when repeating the calculation for warmer days of the year. Although approximate, this calculation shows an operational advantage of the heat pump over the boiler, which offsets the higher unit capital cost. Even greater benefits provided by heat pumps are observed in terms of carbon emissions. Consider a specific emission coefficients of 0.137 and 0.237 ton_{CO_2}/MWh for electricity and gas, respectively. Dividing these emission coefficients by the average efficiencies results in an average emission of 0.258 and 0.060 ton_{CO_2}/MWh for the thermal energy generated by the boiler and the heat pump, respectively. Finally, note that the economic and environmental impacts of heat pumps are further reduced when using solar electricity, suggesting a significant potential for the electrification of the energy system under investigation (no natural gas is imported for emission reductions greater than 10–20%). A similar logic explains the absence of fuel cells and micro gas turbines.

iv. With respect to the storage technologies (Fig. 12e–g), thermal storage is installed along the entire Pareto set, with a larger size for lower CO_2 emissions and higher renewable installation. Note that the thermal storage system also helps to satisfy the thermal demand below the heat pump operation limit (commercial heat pumps can typically operate between 10% and 100% of the rated power). On the contrary, battery and power-to-gas systems are only selected at high emission reductions, due to the necessity to fully exploit the renewable generation. Going from low cost to low emissions, the battery is the first to be installed due to the lower installation cost and the higher round-trip efficiency on short-term periods. Then, at very high emission reductions (greater than 80–90%), where a seasonal compensation of the renewable generation is necessary, the PtG system is installed due to higher round-trip efficiency on long-term periods.

v Independently of the area available for solar generation, the electrical grid plays a relevant role along the entire Pareto front (Fig. 12h). For the base scenario, even when the maximum solar area is installed (minimum-emission with $A = 6{,}000$ m^2) the imported electricity still accounts for more than half of the overall energy required. This highlights the potential for reduced grid emissions, which is in fact fairly low within the Swiss framework. In contexts characterized by a higher environmental impact of the electrical grid, e.g. US or UK, the decarbonization of the electrical grid could reduce the need for decentralized storage or the necessity for grid-independent energy hubs. The theme of energy autarky in residential applications has been investigated, among others, by McKenna et al. in [62].

The yearly operation of the storage technologies is further

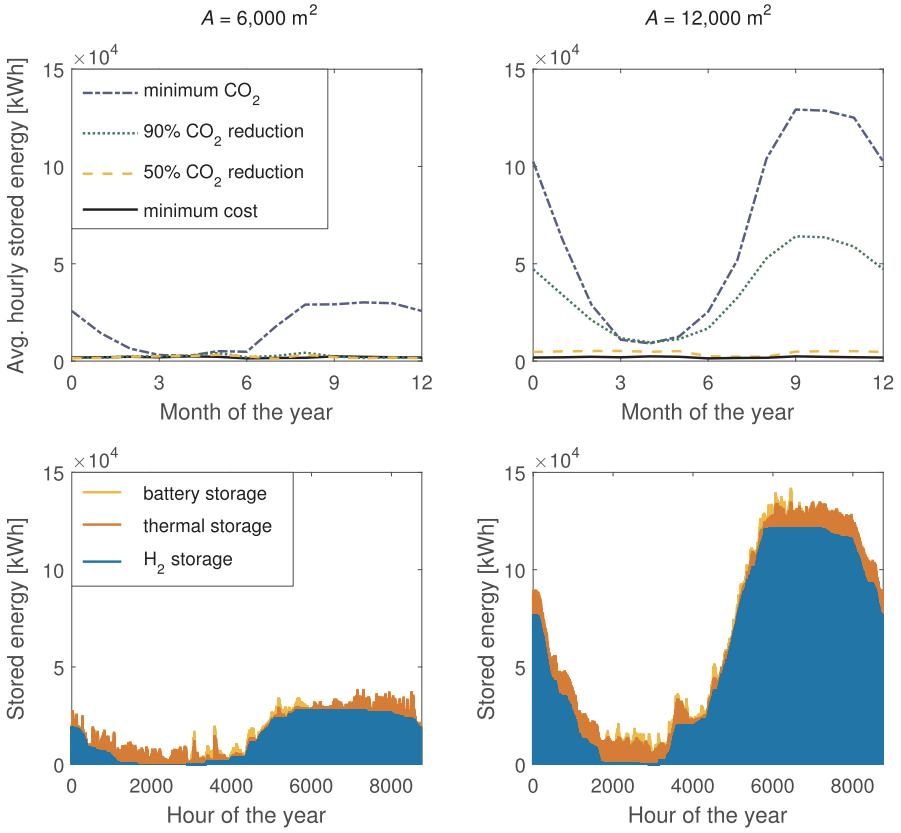

Fig. 13. Left: $A = 6{,}000$ m^2 of available area for solar installation. Right: $A = 12{,}000$ m^2 of available area for solar installation. Top: average hourly value of the total stored energy (LiB, HWTS, HS) during each month of the year for various scenarios: minimum-cost (solid line), minimum-emission (dot-dash line), 50% CO_2 emission reduction (dashed line), 90% CO_2 emission reduction (dotted line). Bottom: hourly profiles of stored energy for the different technologies for the minimum-emission scenario.

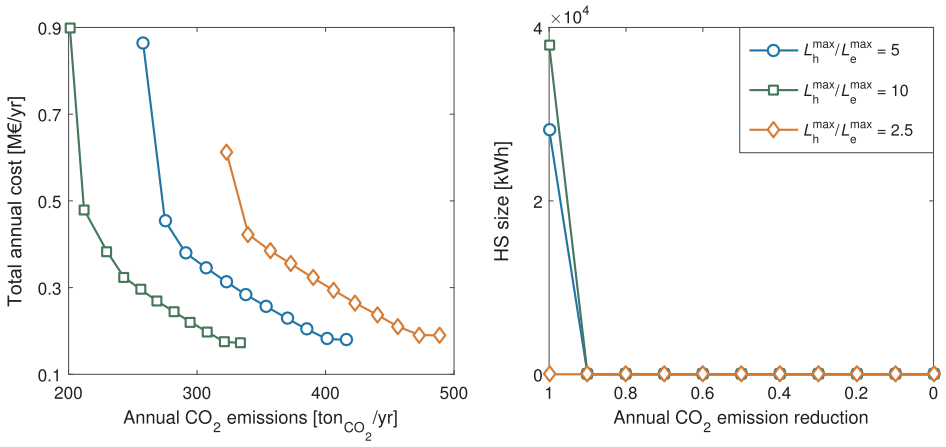

Fig. 14. Left: cost-emission Pareto fronts for three scenarios characterized by different ratios of the maximum thermal to electrical demand: 2.5 (red diamond), 5 (blue circle) and 10 (green square). A ratio equal to 5 corresponds to the reference value based on the input data. Right: size of the hydrogen storage along the three Pareto fronts. (For interpretation of the references to colour in this figure legend, the reader is referred to the web version of this article.)

investigated in Fig. 13. In the top sub-figures, the average hourly value of the total stored energy is reported during each month of the year for (i) the minimum-cost design, (ii) the minimum-emission design, (iii) 50% emission reduction and (iv) 90% emission reduction. The total stored energy is given by the sum of the energy stored in the battery, thermal storage and hydrogen storage systems. In the bottom sub-figures, the contributions of the different storage systems are reported with hour resolution for the minimum-emission scenario. It is worth noticing that the seasonal compensation of renewable generation is not required for emission reductions lower than 90%. In fact, a lower amount of energy is stored in summer until a 60% emission reduction due to the lower thermal demand. Thus, shorter operation cycles, though longer than one week, are implemented in this case by means of the thermal storage system. On the contrary, seasonal operation cycles become optimal for emission reductions above 90%. In this case, the optimal storage system to enable seasonal compensation is the PtG due to the low energy losses of the HS, whereas the battery and the thermal storage system are used for shorter compensation, where their higher round-trip efficiency is rewarded. This difference in storage utilization translates into a maximum installed size for the HS significantly bigger than for HWTS and LiB, though none of the storage technologies reaches the maximum size value (see Table 2) independently of the considered scenarios. Moreover, it is observed that doubling the availability of renewable sources a remarkable increase in seasonal compensation is observed, with the HS growing more than three times with respect to the reference case.

Furthermore, sensitivity analysis is performed to investigate the influence of user demands on the design of the integrated system. In particular, while the overall required energy is kept constant, as well as the shape of the demands, three different values of the ratio between the maximum thermal demand and the maximum electrical demand are considered, namely 2.5, 5 (reference value based on input data) and 10. The results of the analysis are reported in Fig. 14, which shows the Pareto sets (left) and the size of the hydrogen storage (right) for the three cases. On the one hand, it is possible to notice that a higher thermal-to-electrical demand ratio leads to lower CO_2 emissions. This is due to the possibility of converting electrical energy into thermal energy with a heat pump that features an average COP of 3.5 (typical value based on average temperature conditions). On the other hand, this emission reduction comes with a higher total annual cost. This depends on the necessity of installing a power to gas system to store the excess in renewable generation. In fact, the power to gas system is only installed above a certain thermal-to-electrical demand ratio due to the different yearly distributions of the two demands (see Appendix): whereas the electrical demand is fairly constant along the year, the thermal demand exhibits a strong seasonal variation. Seasonal operation cycles are required when a high offset between renewable generation (higher in summer) and demand (higher in winter) is registered, i.e. when the thermal demand is predominant over the electrical demand.

Finally, a sensitivity analysis is conducted on the installation cost of battery and power-to-gas to investigate the impact of a cost reduction

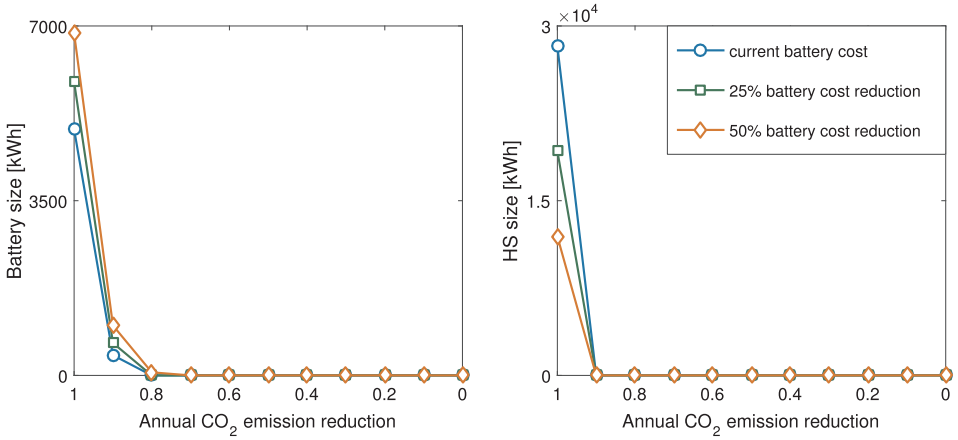

Fig. 15. Left: size of the battery along the Pareto fronts for three scenarios characterized by different battery installation cost: current value (blue circle), 25% reduction (green square) and 50% reduction (red diamond). Right: size of the hydrogen storage along the three Pareto fronts. (For interpretation of the references to colour in this figure legend, the reader is referred to the web version of this article.)

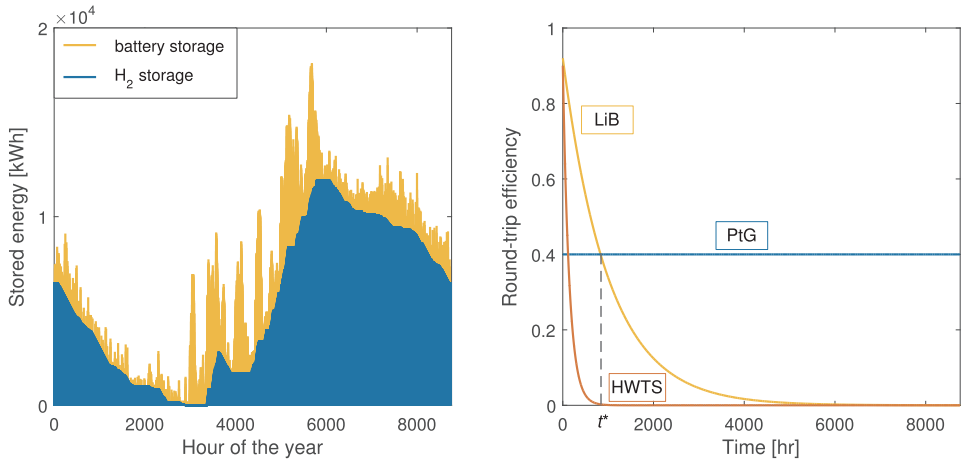

Fig. 16. Left: hourly profiles of the stored energy for LiB (in yellow) and HS (in blue) for the minimum-emission scenario for a 50% reduction of the LiB investment cost. Right: round-trip efficiency of the storage technologies.

on the design of the integrated system. In specific, a cost reduction of 25% and 50% is considered for both technologies with respect to the reference scenario. The cost of the hot water thermal storage is not changed, being this a mature technology. On the one side, reducing the cost of the PtG system does not affect the optimal MES design, as the PtG is always installed at high emission reductions and sized based on the variation between renewable generation and user demand. On the other side, reducing the cost of the battery affects the design of the MES. Results are reported in Fig. 15, showing the size of the battery (left) and the size of the hydrogen storage (right) for the three cases. A reduction in the installation cost of the battery translates into a larger battery installation and a smaller size of the HS, though a certain size of HS is always needed to compensate seasonal variations. Fig. 16 (left) reports the operation of LiB and HS systems along the year for the minimum-emission scenario and a 50% cost reduction. It is observed that although the PtG system represents the higher contribution to seasonal operation, the battery starts being operated with longer-term cycles: from daily cycles during the winter period to weekly and bi-weekly cycles (up to 400 h) during the spring and summer periods, characterized by a higher variation in renewable generation. This operation of the battery system is justified by a round-trip efficiency significantly higher than that of PtG during bi-weekly periods, as illustrated in Fig. 16 (right).

4. Conclusions

This paper presents an optimization framework for the optimal design and operation of multi-energy systems including seasonal energy storage. Two novel MILP models are formulated based on the coupling of typical design days and on the distinction of the decision variables between related and unrelated to binary variables. The proposed approaches allow to consider a year time horizon with hour resolution whilst significantly reducing the computation complexity of the optimization problem.

First, the validity of the proposed techniques are tested by considering a simple multi-energy system that can be solved in a reasonable computation time without resorting to typical days, i.e. through a full scale optimization. In this context, a minimum-cost optimization problem is formulated and the proposed strategies are compared against the full scale optimization and the traditional approach relying on uncoupled design days. Findings show that the proposed approaches provide results in good agreement with the full scale optimization, enabling the design, operation and analysis of complex multi-energy systems involving long-term storage.

Furthermore, the developed tool is applied to perform the multi-objective optimization of a residential multi-energy system including seasonal storage. The results are presented in terms of cost-emission Pareto fronts and underline the possibility of a significant reduction in total annual cost and emissions with respect of traditional systems. The topology of the system along the Pareto sets is presented to reveal the behavior of the system and to identify the potential of the investigated technologies for different emission levels and for different boundary conditions. In particular, it is observed that seasonal operation cycles become convenient when a significant reduction in CO_2 emission is required. Moreover, they are favored when a large amount of renewable generation is available and when the system is characterized by a large ratio of thermal to electrical demand. Finally, a remarkable potential for the electrification of the system under investigation, as well as a relevant role of the electricity grid, are observed.

Acknowledgements

This work was supported by the Swiss National Science Foundation (SNF) under the National Research Program Energy Turnaround (NRP70), Grant No. 407040-153890. Dr. Martelli acknowledges LEAP (Laboratorio Energia Ambiente Piacenza) and the Efficity project (CUP E38I16000130007) co-funded by Regione Emilia Romagna.

Appendix A

The reference sets of input data used in this work, namely the hourly profile of the solar radiation, the ambient temperature, the electricity price,

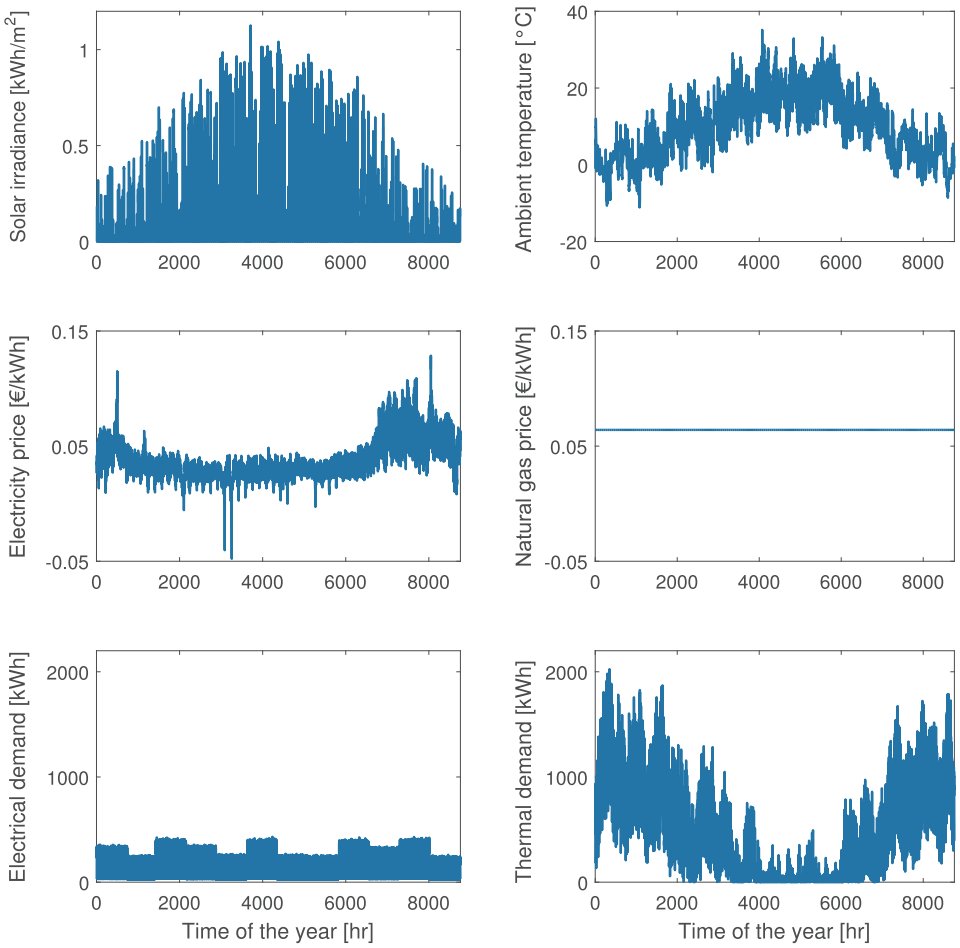

Fig. 17. Reference sets of input data: solar irradiance, ambient temperature, electricity price, natural gas price, electrical demand, thermal demand.

the natural gas price, the electrical demand, the thermal demand, are reported in Fig. 17.

Appendix B. Supplementary material

Supplementary data associated with this article can be found, in the online version, at http://dx.doi.org/10.1016/j.apenergy.2017.07.142.

References

[1] IPCC. Climate Change 2013: The Physical Science Basis (Summary for Policymakers); 2013.
[2] Mancarella Pierluigi. MES (multi-energy systems): an overview of concepts and evaluation models. Energy 2014;65:1–17.
[3] Pinel Patrice, Cruickshank Cynthia A, Beausoleil-Morrison Ian, Wills Adam. A review of available methods for seasonal storage of solar thermal energy in residential applications. Renew Sustain Energy Rev 2011;15(7):3341–59.
[4] Alarcon-Rodriguez Arturo, Ault Graham, Galloway Stuart. Multi-objective planning of distributed energy resources: a review of the state-of-the-art. Renew Sustain Energy Rev 2010;14(5):1353–66.
[5] Connolly D, Lund H, Mathiesen BV, Leahy M. A review of computer tools for analysing the integration of renewable energy into various energy systems. Appl Energy 2010;87(4):1059–82.
[6] Keirstead James, Jennings Mark, Sivakumar Aruna. A review of urban energy system models: approaches, challenges and opportunities. Renew Sustain Energy Rev 2012;16(6):3847–66.
[7] Allegrini Jonas, Orehounig Kristina, Mavromatidis Georgios, Ruesch Florian, Dorer Viktor, Evins Ralph. A review of modelling approaches and tools for the simulation of district-scale energy systems. Renew Sustain Energy Rev 2015;52:1391–404.
[8] Elsido Cristina, Bischi Aldo, Silva Paolo, Martelli Emanuele. Two-stage MINLP algorithm for the optimal synthesis and design of networks of CHP units. Energy 2017;121:403–26.
[9] Marnay Chris, Venkataramanan Giri, Stadler Michael, Siddiqui Afzal, Firestone Ryan, Chandran Bala. Optimal technology selection and operation of commercial-building microgrids. IEEE Trans Power Syst 2007;23(3):1–10.
[10] Hawkes AD, Leach MA. Modelling high level system design and unit commitment for a microgrid. Appl Energy 2009;86(7–8):1253–65.
[11] Angrisani G, Roselli C, Sasso M. Distributed microtrigeneration systems. Prog Energy Combust Sci 2012;38(4):502–21.
[12] Fazlollahi Samira, Mandel Pierre, Becker Gwenaelle, Maréchal Francois. Methods for multi-objective investment and operating optimization of complex energy systems. Energy 2012;45(1):12–22.
[13] Ahmadi Pouria, Rosen Marc A, Dincer Ibrahim. Multi-objective exergy-based optimization of a polygeneration energy system using an evolutionary algorithm. Energy 2012;46(1):21–31.
[14] Genon Giuseppe, Torchio Marco F, Poggio Alberto, Poggio Marco. Energy and environmental assessment of small district heating systems: global and local effects in two case-studies. Energy Convers Manage 2009;50(3):522–9.
[15] Weber C, Shah N. Optimisation based design of a district energy system for an eco-town in the United Kingdom. Energy 2011;36(2):1292–308.
[16] Mehleri Eugenia D, Sarimveis Haralambos, Markatos Nikolaos C, Papageorgiou Lazaros G. A mathematical programming approach for optimal design of distributed energy systems at the neighbourhood level. Energy 2012;44(1):96–104.
[17] Mehleri Eugenia D, Sarimveis Haralambos, Markatos Nikolaos C, Papageorgiou Lazaros G. Optimal design and operation of distributed energy systems: application to Greek residential sector. Renew Energy 2013;51:331–42.
[18] Omu Akomeno, Choudhary Ruchi, Boies AM. Distributed energy resource system optimisation using mixed integer linear programming. Energy Policy 2013;61:249–66.
[19] Bracco Stefano, Dentici Gabriele, Siri Silvia. Economic and environmental optimization model for the design and the operation of a combined heat and power distributed generation system in an urban area. Energy 2013;55:1014–24.
[20] Henning Dag, Amiri Shahnaz, Holmgren Kristina. Modelling and optimisation of

electricity, steam and district heating production for a local Swedish utility. Eur J Oper Res 2006;175(2):1224–47.
[21] Siddiqui Afzal S, Firestone Ryan, Ghosh Srijay, Stadler Michael, Edwards Jennifer L, Marnay Chris. Customer adoption modeling with combined heat and power applications. Technical report LBNL-52718, Lawrence Berkeley National Laboratory; 2003.
[22] Stadler M, Groissböck M, Cardoso G, Marnay C. Optimizing Distributed Energy Resources and building retrofits with the strategic DER-CAModel. Appl Energy 2014;132:557–67.
[23] Steen David, Stadler Michael, Cardoso Gonçalo, Groissböck Markus, DeForest Nicholas, Marnay Chris. Modeling of thermal storage systems in MILP distributed energy resource models. Appl Energy 2015;137:782–92.
[24] Clegg Stephen, Mancarella Pierluigi. Storing renewables in the gas network: modelling of power-to-gas seasonal storage flexibility in low-carbon power systems. IET Gener, Transmiss Distrib 2016;10(3):566–75.
[25] Sahinidis Nikolaos V. Optimization under uncertainty: state-of-the-art and opportunities. Comput Chem Eng 2004;28(6-7):971–83.
[26] Wallace Stein W, Fleten Stein-Erik. Stochastic programming models in energy. Handbooks Oper Res Manage Sci 2003;10:637–77.
[27] Schulze M, Granado PC Del. Optimization modeling in energy storage applied to a multi-carrier system. … Energy Soc Gener Meet … 2010:1–7.
[28] Conejo Antonio J, Carrion Miguel, Morales Juan M. Decision making under uncertainty in electricity markets. Springer; 2010.
[29] Sobu Ango, Wu Guohong. Dynamic optimal schedule management method for microgrid system considering forecast errors of renewable power generations. In: 2012 IEEE international conference on power system technology, POWERCON 2012; 2012.
[30] Chen Zhi, Wu Lei, Fu Yong. Real-time price-based demand response management for residential appliances via stochastic optimization and robust optimization. IEEE Trans Smart Grid 2012;3(4):1822–31.
[31] Arabali Amirsaman, Ghofrani Mahmoud, Etezadi-Amoli Mehdi, Fadali Mohammed Sami. Stochastic performance assessment and sizing for a hybrid power system of Solar/Wind/Energy Storage. IEEE Trans Sustain Energy 2014;5(2):363–71.
[32] Morales Juan Miguel, Conejo Antonio J, Madsen Henrik, Pinson Pierre. Integrating renewables in electricity markets: operational problems. 1st ed. US: Springer; 2014.
[33] Yokoyama Ryohei, Shinano Yuji, Taniguchi Syusuke, Ohkura Masashi, Wakui Tetsuya. Optimization of energy supply systems by MILP branch and bound method in consideration of hierarchical relationship between design and operation. Energy Convers Manage 2015;92:92–104.
[34] De Soto W, Klein SA, Beckman WA. Improvement and validation of a model for photovoltaic array performance. Sol Energy 2006;80(1):78–88.
[35] TVP Solar. <http://www.tvpsolar.com/>.
[36] Climaveneta Global. <https://www.climaveneta.com/EN/>.
[37] Johnson RK. Measured performance of a low temperature air source heat pump. Technical report September, US Department of Energy; 2013.
[38] Glover Fred. Improved linear integer programming formulations of nonlinear integer problems. Manage Sci 1975;22(4):455–60.
[39] Sheikhi A, Ranjbar AM, Oraee H. Financial analysis and optimal size and operation for a multicarrier energy system. Energy Build 2012;48:71–8.
[40] Tesla Motors. <https://www.tesla.com/>.
[41] Smolinka Tom(Fraunhofer Ise), Günther Martin (Fraunhofer Ise), Garche Jürgen (Fcbat). Stand und Entwicklungspotenzial der Wasserelektrolyse zur Herstellung von Wasserstoff aus regenerativen Energien. NOW-Studie, 2010:53, 2011.
[42] Haelg Leonore. Thermal energy storage with combined heat and power. PhD thesis, ETH Zurich; 2014.
[43] Capstone Turbine Corporation. <http://www.capstoneturbine.com/>.
[44] Gabrielli Paolo, Flamm Ben, Eichler Annika, Gazzani Matteo, Lygeros John, Mazzotti Marco, et al. Modeling for optimal operation of PEM fuel cells and electrolyzers. 2016 IEEE 16th international conference on environment and electrical engineering (EEEIC). IEEE; 2016. p. 1–7.
[45] Gabrielli Paolo, Gazzani Matteo, Mazzotti Marco. Modeling fuel cells in integrated multi-energy systems. Energy Proc 2017.
[46] Arroyo José M, Conejo Antonio J. Modeling of start-up and shut-down power trajectories of thermal units. IEEE Trans Power Syst 2004;19(3):1562–8.
[47] Cabeza Luisa Flora, editor. Advances in thermal energy storage systems. Woodhead Publishing; 2015.
[48] Marquant Julien F, Omu Akomeno O, Orehounig Kristina, Evins Ralph, Carmeliet Jan. Application of spatial-temporal clustering to facilitate energy system modeling. Build Simul Conf 2015:551–8.
[49] Keirstead James, Samsatli Nouri, Shah Nilay, Weber Céline. The impact of CHP (combined heat and power) planning restrictions on the efficiency of urban energy systems. Energy 2012;41(1):93–103.
[50] Bracco Stefano, Dentici Gabriele, Siri Silvia. DESOD: a mathematical programming tool to optimally design a distributed energy system. Energy 2016;100:298–309.
[51] Kong Dong-Seok, Jang Yong-Sung, Huh Jung-Ho. Method and case study of multiobjective optimization-based energy system design to minimize the primary energy use and initial investment cost. Energies 2015;8(6):6114–34.
[52] International Energy Agency. Technology roadmap: energy-efficient buildings: heating and cooling equipment. Technical report, International Energy Agency; 2014.
[53] Körner Alexander. Technology roadmap: hydrogen and fuel cells. Technical report, International Energy Agency; 2015.
[54] Hoppmann Joern, Volland Jonas, Schmidt Tobias S, Hoffmann Volker H. The economic viability of battery storage for residential solar photovoltaic systems - a review and a simulation model. Renew Sustain Energy Rev 2014;39:1101–18.
[55] Beccali M, Brunone S, Finocchiaro P, Galletto JM. Method for size optimisation of large wind-hydrogen systems with high penetration on power grids. Appl Energy 2013;102:534–44.
[56] GME. <http://www.mercatoelettrico.org>.
[57] EWZ. <https://www.ewz.ch/de/private>.
[58] Pfenninger Stefan. Dealing with multiple decades of hourly wind and PV time series in energy models: a comparison of methods to reduce time resolution and the planning implications of inter-annual variability. Appl Energy 2017;197:1–13.
[59] MATLAB 8.6.0. Statistics and Machine Learning Toolbox; 2015.
[60] Lloyd S. Least squares quantization in PCM in IEEE Transaction on Information. Theory It-28 I 1982(2):129–37.
[61] IBM. CPLEX ILOG; 2016.
[62] McKenna Russell, Merkel Erik, Fichtner Wolf. Energy autonomy in residential buildings: a techno-economic model-based analysis of the scale effects. Appl Energy 2017.